The Astronomical Journal, 135:2279–2286, 2008 June doi:10.1088/0004-6256/135/6/2279

STAR FORMATION IN THE SOUTHERN DARK CLOUD DC 296.2−3.6

P. Persi[1], M. Gómez[2], M. Tapia[3], M. Roth[4], J. M. De Buizer[5,6], and A. R. Marenzi[1]
[1] INAF–IASF-Roma, Via Fosso del Cavaliere, 100, 00133 Roma, Italy; paolo.persi@iasf-roma.inaf.it
[2] Observatorio Astronómico de Córdoba, Córdoba, Argentina
[3] Instituto de Astronomía, Universidad Nacional Autónoma de México, Ensenada, B.C., Mexico
[4] Las Campanas Observatory, Carnegie Institution of Washington, La Serena, Chile
[5] Gemini Observatory, La Serena, Chile
[6] SOFIA-USRA, NASA Ames Research Center, Moffet Field, CA, USA
Received 2008 February 2; accepted 2008 March 13; published 2008 May 13

ABSTRACT

We report near- and mid-infrared (IR) images of the southern hemisphere dark cloud DC 296.2−3.6 associated with IRAS 11431−6516. The K_s and L' images show the presence of an IR nebulosity at the center of the dark cloud (DC). From the analysis of the near-IR color–color diagrams we have identified a young stellar population in the region. Five of these young stellar objects, here named A, B, C, D, and E, were also detected in the mid-IR. Sources B, D, and E are Class I–II T Tauri as suggested by the analysis of their spectral energy distributions. In addition, source E shows a long-term near-IR variability. The near-IR color–color diagrams indicate the presence of circumstellar dust envelope in sources A, B, D, and E, while the fit of SEDs of the intermediate- and low-mass objects A and B with a radiation transfer model including infalling envelope+disk+central source suggests circumstellar disks around these two objects. These results indicate that DC 296.2−3.6, located in the far Carina arm, is associated with an embedded cluster of low-mass young stellar objects.

Key words: infrared: ISM – ISM: clouds – stars: formation – stars: individual (DC 296.2−3.6)

1. INTRODUCTION

In general, dark clouds (DCs) are defined as regions where the apparent surface density of stars is much lower than that of the surrounding areas. Two complete catalogs of DCs have been published by Lynds (1962) and Hartley et al. (1986) covering the entire sky. Both catalogs have become basic references for studies involving possible sites of star formation and have been the subject of observations at all wavelength ranges.

The Southern Hemisphere catalog of Hartley et al. (1986) contains 1101 DCs with $\delta \leqslant -33^\circ$ of which approximately 50% have small sizes ($\leqslant$64 arcmin^2) and *IRAS* sources within their boundaries (Persi et al. 1990). A survey in the NH_3 (1, 1) line of 169 southern small and isolated DCs (globules) with diameters less than 10′ was undertaken by Bourke et al. (1995), in order to determine the physical characteristics of these regions. A systematic search for millimeter dust continuum emission and CO molecular outflows from 35 southern small DCs associated with cold *IRAS* sources was done by Henning & Launhardt (1998). Continuum emission at 1.3 mm was detected in 18 clouds, and in 12 clouds the CO line wings indicated the presence of molecular outflows. All these observations show that a number of small DCs from Hartley et al.'s catalog are active centers of star formation, especially of low-mass stars. Preliminary results of a new infrared (IR) study of 14 southern DCs have been reported by Persi et al. (2007).

DC 296.2−3.6 is a mean-density cloud (class B in the nomenclature of (Hartley et al. 1986)) that is associated with a reflection nebula. The *IRAS* source 11431−6516 with colors typical of a core-type source is embedded in this DC (Persi et al. 1990). The region is also reported in the catalog of southern hemisphere nebulosities as BWW 371 (Brand et al. 1986). Brand & Blitz (1993) determined its kinematical distance of 3.6 kpc that locates this cloud in the far Carina arm (2.2 kpc $\leqslant d \leqslant$ 4.4 kpc). Continuum emission at 1.3 mm, and of the CO (J = 2–1) and CS (J = 2–1) lines were detected by Henning & Launhardt (1998) using a large beam (23″). From the *IRAS* flux densities and the observed 1.3 mm emission, these authors determined a bolometric luminosity of $L = 1.3 \times 10^4 L_\odot$ and $M_{\rm gas} = 37 M_\odot$ beam^{-1} for this globule. Because of their large distances, Henning & Launhardt (1998) proposed that these DCs with *IRAS* sources in the far Carina arm are not typical classical globules. According to their masses and luminosities, they are probably associated with embedded clusters of low- (or intermediate-) mass young stellar objects (YSOs) devoid of high-mass stars.

In order to search for possible embedded low-mass YSOs in the far Carina dark cloud DC 296 2−3.6, we have obtained high-resolution near- and mid-IR observations, described in Section 2. We discuss in Section 3 the near-IR color–color plots to discriminate field stars from embedded sources. In addition, the spectral energy distributions (SEDs) of the newly detected mid-IR sources are presented and compared with the model described by Robitaille et al. (2007). Finally, Section 4 lists our conclusions.

2. OBSERVATIONS

2.1. Near-Infrared Images

The new near-IR images of DC 296.2−3.6 were obtained at two different epochs at Las Campanas Observatory in Chile. A different combination of telescope and instrument was used during each run.

On 1999 January 5 and 7, we used the near-IR camera IRCAM (Persson et al. 1992) attached to the 2.5 m du Pont telescope. A mosaic was constructed for each of the J-, H-, and K_s-bands from five overlapping frames covering an area of 90″ × 90″ centered at the *IRAS* position. The total exposure times were 1000 s, 800 s, and 500 s for J, H, and K_s, respectively. The adopted image scale was 0.35″ pixel^{-1} and the observed range of point-spread functions (PSFs) was 0.8″–1.0″ (FWHM). Flux calibration was done by observing standard stars from the list of

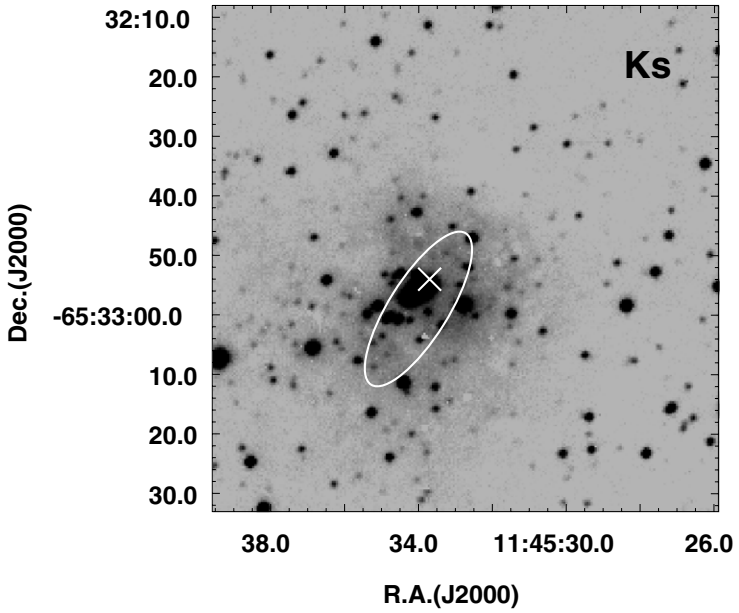

Figure 1. K_s image of DC 296.2−3.6 taken with the 2.5 m du Pont telescope. The ellipsoid marks the *IRAS* positional uncertainties, and the symbol × represents the position of the *MSX* source associated with this cloud.

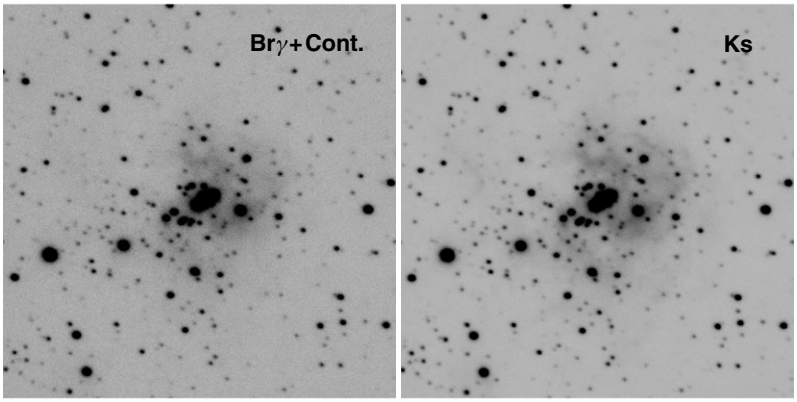

Figure 2. Comparison between Brγ and the normalized K_s image of DC 296.2−3.6.

Las Campanas Observatory. Stellar photometry was performed using the DAOPHOT package (Stetson 1987) within IRAF with an aperture of 3″. With the adopted total exposure time we measured detection limits of 19.1, 18.3, and 17.5 mag (3σ) at J, H, and K_s, respectively. Star positions were determined using a grid of stars included in the *HST* Guide Star Catalogue. The K_s image taken with IRCAM shows an IR nebulosity just at the center of the *IRAS* ellipsoid (Figure 1).

This DC was also observed, with higher sensitivity and better seeing conditions, using Persson's Auxiliary Nasmyth Infrared Camera (PANIC) attached to the Magellan Baade 6.5 m telescope on 2007 April 10. PANIC uses a Hawaii 1024 × 1024 HgCdTe array that provides a 2′ × 2′ field of view with a scale of 0.125″ pixel^{-1}. It has identical J, H, and K_s broadband filters as IRCAM. We obtained nine dithered 50 s exposure frames offsetting 6″ between positions. The measured PSF (FWHM) was 0.6″–0.7″ in the K_s-band. These near-IR images are approximately 1.6 mag deeper than those obtained with the du Pont telescope. Flux calibration and photometry were performed as described above but with a 1.25″ aperture. Additionally, an image of the same field was taken with PANIC through a narrowband filter centered in the Brγ line (λ_o = 2.165 μm, $\Delta\lambda$ = 0.0224 μm). In this case, the exposure time per dithered frame was 90 s. Figure 2 illustrates the comparison between the Brγ image and the normalized K_s image. From this comparison, it appears evident that no significant hydrogen line emission arises from any region of the field.

Figure 3 shows a composite "true-color" picture (J, H, and K_s in blue, green, and red, respectively) of DC 296.2−3.6 from the near-IR images obtained with PANIC on the 6.5 m telescope. It covers an area of 126″ × 126″.

2.2. L' and Mid-Infrared Images

An L' (λ_o = 3.78 μm, $\Delta\lambda$ = 0.57 μm) image centered on IRAS 11431−6516 was retrieved from the ESO archive. This observation was made on 2000 June 19, in service mode, with the ISAAC camera (Moorwood et al. 1998) mounted on Unit 1 (Antu) of the ESO Very Large Telescope (VLT). The ISAAC camera provides a scale of 0.07″ pixel^{-1}. The observations were

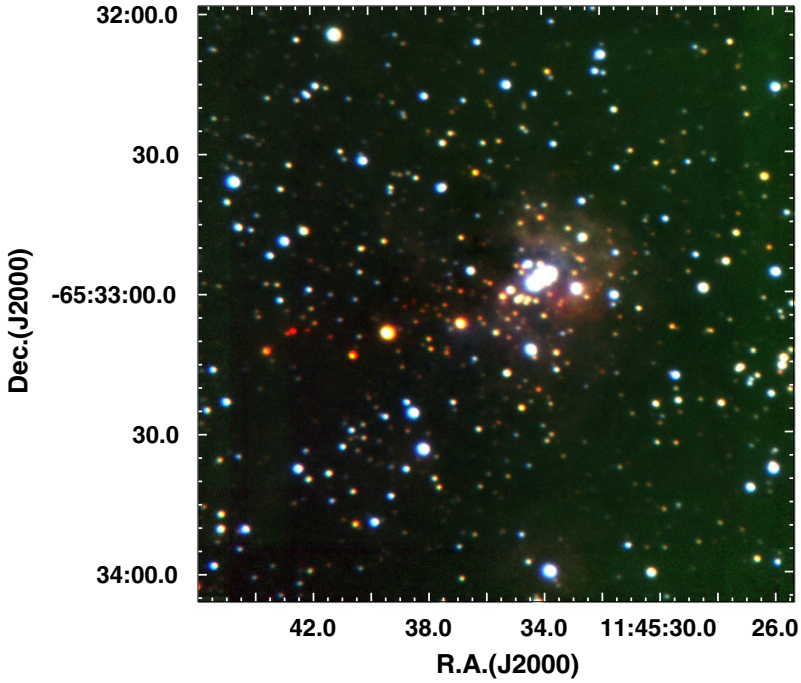

Figure 3. "True-color" image made from the J (blue), H (green), and K_s (red) individual Baade's images in an area of 126″ × 126″ of DC 296.2−3.6.

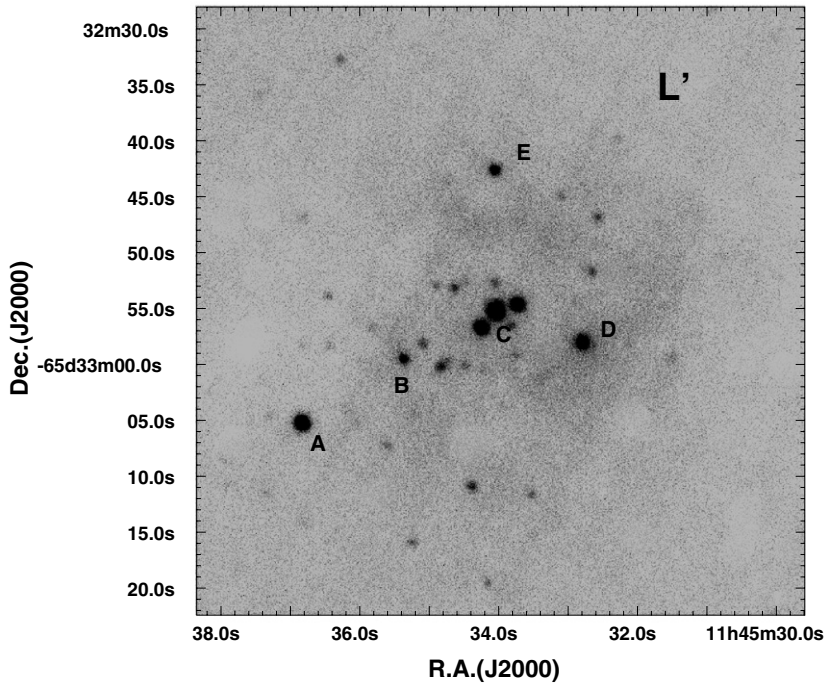

Figure 4. ISAAC L' image of DC 296.2−3.6 (IRAS 11431−6516) from the ESO archive.

carried out in the chopping and nodding mode, with the chopping throw of 30″ in declination (decl.) at a frequency of 0.43 Hz. The standard star HR 6736 was used to flux calibrate the image. The photometry of the detected sources was performed as for the near-IR images with an aperture of 1.2″. The ISAAC L'-band image of DC 296.2−3.6 is reported in Figure 4.

Mid-IR images taken through the N (7.07−12.97 μm) and Q_a (17.07−19.08 μm) filters were carried out with the Gemini South telescope using the Thermal-Region Camera and Spectrograph (T-ReCS) on the night of 2007 February 13. The instrument employs a Raytheon 320 × 240 pixel Si:As Blocked Impurity Band (BIB) array with a pixel scale of 0.089″ pixel^{-1}, yielding a field of view of size 28.5″ × 21.4″. Sky and telescope subtraction were achieved through the standard chop-nod technique. The images were flux-calibrated observing the standard star HD 91056 assuming flux densities at N of

Table 1
Coordinates and IR Photometry of the Five Mid-IR Sources

Source	R.A.(J2000) h m s	Decl.(J2000) ° ′ ″	J (mag)	H (mag)	K_s (mag)	L' (mag)	$F_\nu(N)$ (mJy)	$F_\nu(Q_a)$ (mJy)
DC 296.2−3.6(A)	11 45 36.9	−65 33 06	16.57	13.90	12.09	9.58	203.6(5.5)	941.4(56.2)
DC 296.2−3.6(B)	11 45 35.4	−65 33 01	16.99	15.30	13.83	11.12	60.6(4.0)	164.5(14.3)
DC 296.2−3.6(C)	11 45 34.1	−65 32 56	13.91	12.65	11.59	9.09	16.9(1.9)	$\leqslant$12.3
DC 296.2−3.6(D)	11 45 32.9	−65 32 59	14.37	13.30	12.51	10.36	40.6(3.2)	497.1(35.1)
DC 296.2−3.6(E)	11 45 34.1	−65 32 44	18.34	16.51	14.71	10.81	24.6(1.8)	47.0(12.2)

Note. The numbers in the parentheses represent the 1σ statistical errors in the mid-IR fluxes.

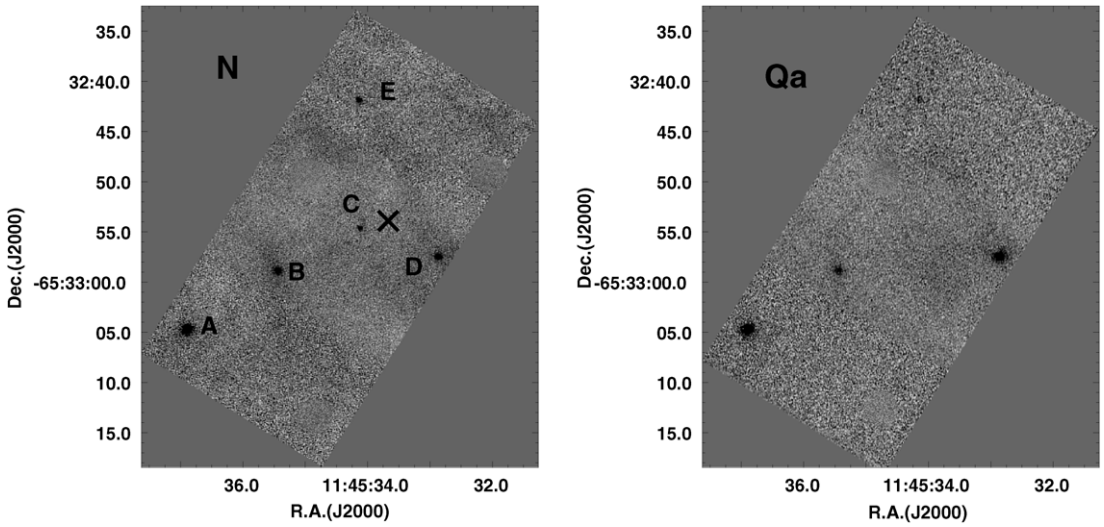

Figure 5. Mid-IR images in the N and Q_a bands obtained with T-ReCS at the Gemini South telescope. The positions of the five mid-IR sources (A–E) are reported. The symbol × indicates the position of the *MSX* source.

24.486 Jy and Q_a of 8.686 Jy. These were determined by convolving the spectral irradiance template of the star from Cohen et al. (1999) with the given T-ReCS filter transmission profile. In a mosaic of size 39″ × 46″, we detected five mid-IR sources in N and four in Q_a, which we named A, B, C, D, and E (see Figure 5). All these mid-IR sources have also been detected in the J, H, K_s, and in the L' broadbands as shown in Figure 4. Their coordinates and magnitudes are given in Table 1. The near-IR magnitudes reported here are from the photometry of the Baade images. The estimated position uncertainties of the sources in Table 1 is 1″.

3. DISCUSSION

3.1. Color–Color Diagrams

In order to study the nature of the IR sources in DC 296.2−3.6, we have analyzed the $J-H$ versus $H-K_s$ and the $H-K_s$ versus $K_s - L'$ color–color diagrams from our PANIC and ISAAC photometry. In an area of size 144″ × 144″ around the *IRAS* position, we detected 631 sources in K_s, 600 in H, and 581 in J within our quoted sensitivity, while 28 sources were detected in L' at a limit of 13.5 mag (3σ) in a smaller area (54″ × 54″). Figures 6 and 7 illustrate the color–color diagrams constructed from measurements with errors smaller than 0.2 mag in the three colors. After considering the photometric errors, the location of most sources in the $J - H$ versus $H - K_s$ plot (Figure 6) is consistent with normal reddened stars with A_V ranging from 5 to 15 mag. Nevertheless, approximately 20–30 of the near-IR sources including the five mid-IR sources A, B, C, D, and E

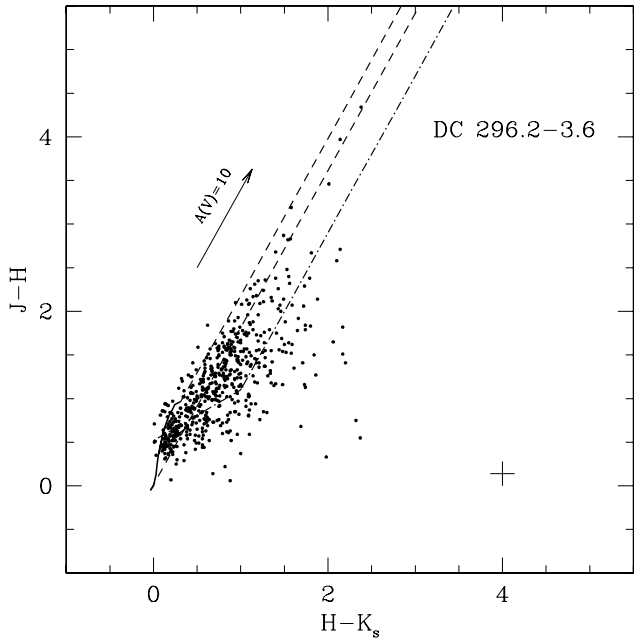

Figure 6. $J - H$ versus $H - K_s$ diagram. The solid line marks the loci of the main-sequence (MS) stars from Bessel & Brett (1988) while the dashed lines define the reddening band extending from the MS using the reddening vector from Rieke & Lebofsky (1985). The dot-dashed line represents the colors of un-reddened classical T Tauri stars (Meyer et al. 1997). The symbol + indicates the mean statistical error.

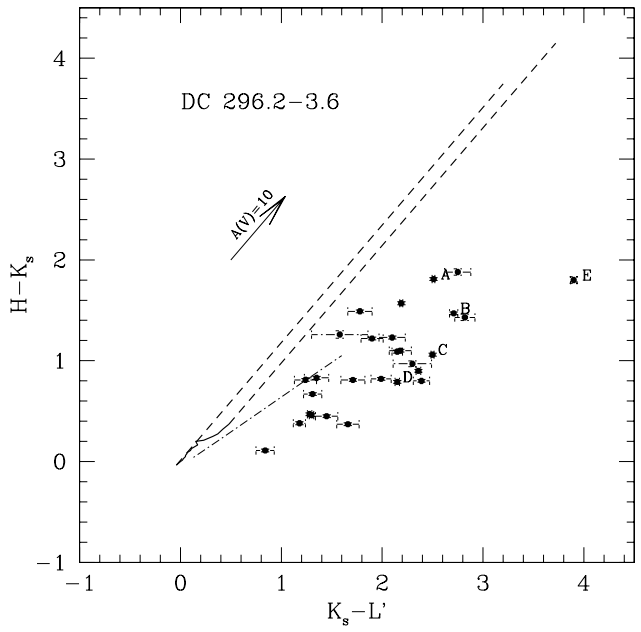

Figure 7. $H - K_s$ versus $K_s - L'$ diagram. The solid and dashed lines as in Figure 6. The dot-dashed line represents the colors of un-reddened classical T Tauri stars from Meyer et al. (1997) who found that for higher accretion rates the slope of this line decreases considerably.

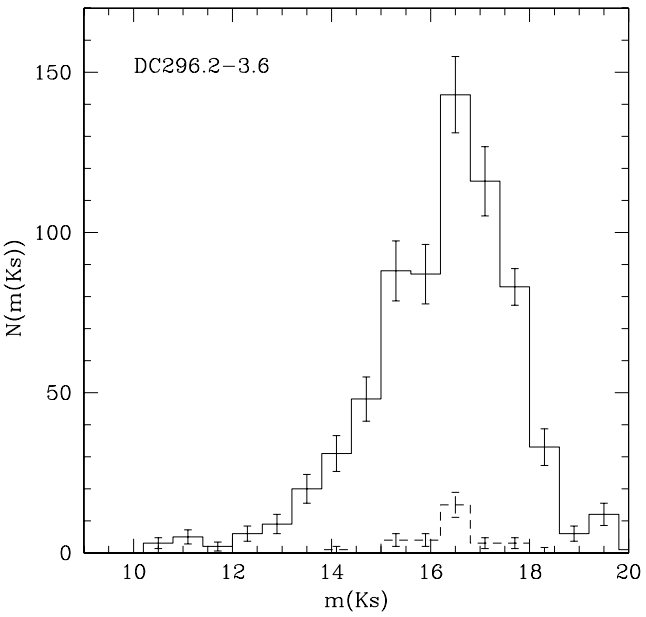

Figure 8. K_s magnitude distribution of the 631 sources detected in an area of 144″ × 144″ in DC 296.2−3.6. The dashed line shows the K_s distribution of the sources with near-IR excess. The error bars correspond to the statistical errors for each bin.

show significant IR excess. This is confirmed by the location of these sources on the $H - K_s$ versus $K_s - L'$ diagram (see Figure 7). These IR excesses are interpreted as evidence of the presence of dust circumstellar envelopes or disks around these objects.

The K_s magnitude distribution of all detected sources in DC 296.2−3.6 compared with the sources with near-IR excess is reported in Figure 8. Both distributions peak at around K_s = 16.5 mag. Assuming a distance modulus of $m - M = 12.78$ ($d = 3.6$ kpc), $A_K = 1.1$, this corresponds to $M_K = 2.6$. The

Table 2
IR Luminosities and IR Spectral Indices for the Five Mid-IR Sources

Source	L(IR) ($L_\odot$)	α(IR)
DC 296.2−3.6(A)	58.5	0.91
DC 296.2−3.6(B)	12.5	1.16
DC 296.2−3.6(C)	3	−0.96
DC 296.2−3.6(D)	13.4	0.13
DC 296.2−3.6(E)	5.6	1.10

Table 3
Physical Parameters of Sources A and B Derived from the Robitaille et al. (2007) R07 Model

Parameters	A	B
Stellar mass ($M_\odot$)	4.14	0.58
Stellar temperature (K)	4385	3757
Envelope accretion rate ($M_\odot$ yr^{-1})	3.1×10^{-5}	1.8×10^{-4}
Envelope outer radius (AU)	9.5×10^{3}	2.5×10^{3}
Disk mass ($M_\odot$)	4.4×10^{-3}	3.4×10^{-3}
Disk outer radius (AU)	2.1×10^{2}	8.6
Disk inner radius (AU)	2.6	0.4
Disk accretion rate ($M_\odot$ yr^{-1})	6.3×10^{-3}	1.5×10^{-3}
Inclination (°)	31.8	18.2
A_V	30.6	45.0
Total luminosity ($L_\odot$)	143	41

result indicates the presence in the DC of a cluster of late-type YSOs, located in an area of approximately 30″ × 30″ around the *IRAS* position (Figure 9).

3.2. Spectral Energy Distributions (SEDs)

We have derived the SEDs of sources A–E (Figures 10 and 11) from the IR photometry of Table 1. For sources A, B, D, and E we also plotted their Two Micron All Sky Survey (2MASS) photometry (open squares in Figure 11) as well as that from the du Pont telescope (open triangles in Figure 11), all taken at different epochs. Sources A, B, and D do not show any near-IR variability within the quoted statistical errors. On the other hand, the comparison of the 1999 ($J = 16.73(0.10)$, $H = 15.23(0.05)$, and $K_s = 14.04(0.04)$) and 2007 mag of source E (see Table 1) indicates a near-IR variability typical of young T Tauri stars.

Integrating the SEDs of Figures 10 and 11 from 1 to 18 μm we have determined the IR luminosities and we have computed the IR spectral indices $\alpha_{\rm IR}(2.2\text{–}10.3\ \mu{\rm m}) = d \log \lambda F_\lambda / d \log \lambda$ using the observed 2.2 and 10.3 μm flux densities. The resulting spectral indices, reported in Table 2, suggest that sources B, D, and E are probably embedded Class I–II T Tauri stars. The negative α(IR) observed in source C could be interpreted as due to a Class III source, but this is in contrast with the observed IR excess in the L'-band. Finally, source A might be an intermediate-mass young star, based on its high luminosity.

The infalling envelope+disk+central source radiation transfer model described by Robitaille et al. (2007) (R07) has been used to fit the observed SED of sources A and B only. Source D shows an unusual IR SED with a flat spectrum between 1 and 10 μm and a very steep rise between 10 and 18 μm, while source E shows considerable variations in the IR (see Figure 11). The continuous lines of Figure 12 show the best-fit models obtained using the SED fitting tool by Robitaille et al. (2007) (R07). The derived physical parameters are summarized in Table 3. The bolometric luminosities reported here are by a

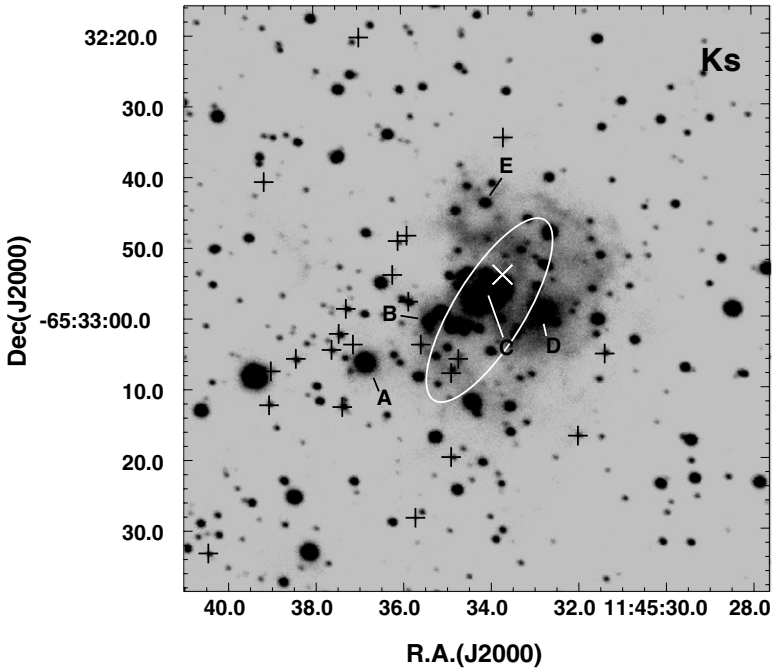

Figure 9. K_s Baade image with the spatial distribution of the sources with near-IR excess (+).

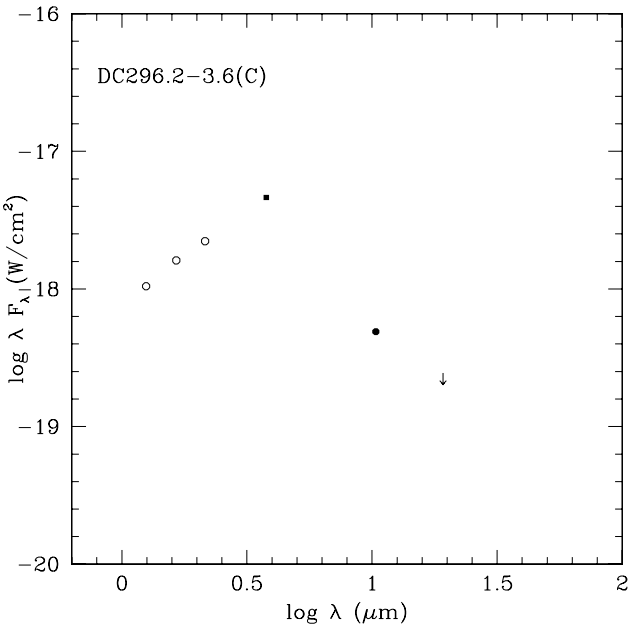

Figure 10. SED of source C in DC 296.2−3.6. The open and filled circles are the observations taken with the Baade and Gemini telescopes, respectively.

factor of 3 greater than the IR luminosities of Table 2. This is due to the fact that their SEDs have rising fluxes beyond 20 μm. Therefore, the luminosities of the sources D and E could also be underestimated. The parameters given in Table 3 are only indicative given the lack of observations in the far-IR and millimeter spectral regions. However, our results clearly indicate the presence of circumstellar disks around these two sources.

Finally, a source is reported in the *Midcourse Space Experiment* (*MSX*) Point Source Catalog (Egan et al. 1999) at R.A.(J2000) = $11^h45^m33\overset{s}{.}8$, decl.(J2000) = $-65°32'56''$ with a position accuracy of $0.6''$. This source lies between C and D, almost at the center of the *IRAS* ellipsoid error (see Figure 1). The observed *MSX* fluxes are [8.28] = 4.96 Jy, [12.13] = 5.79 Jy, and [21.34] = 17.11 Jy, which are much larger than the sum of the five compact sources measured with T-ReCS. Given the fact that the PSF of the *MSX* observations is of the order of $30''$–$40''$, we conclude that there is considerable extended mid-IR emission from DC 296.2−3.6.

4. CONCLUSIONS

We have imaged at high sensitivity and sub-arcsec resolution in the near- and mid-IR the southern hemisphere dark cloud DC 296.2−3.6. From the analysis of these observations we derived the following conclusions:

1. More than 25 near-IR sources with significant excess emission at $\lambda > 2$ μm were found in an area of $\sim 30'' \times 30''$ centered at the *IRAS* position. Their observed K_s magnitude distribution peaks at $M_K = 2.6$, indicated the presence of a cluster of low-mass YSOs. An IR nebulosity surrounding these sources was found, which is particularly bright on the K_s and L' images.
2. Emission in the Brγ was not detected in the field as shown by the comparison between the Brγ image and the normalized K_s continuum (see Figure 2). This implies that no ionized gas is present in the DC.
3. Five unresolved mid-IR sources were found around the center of the DC. Three of these, named B, D, and E, have IR luminosities and spectral indices that are typical of Class I–II T Tauri stars (see Table 2). In addition, source E shows a long-term variability typical of classical T Tauri stars. The intermediate- and low-mass young objects A and B, respectively, have circumstellar disks as indicated by the

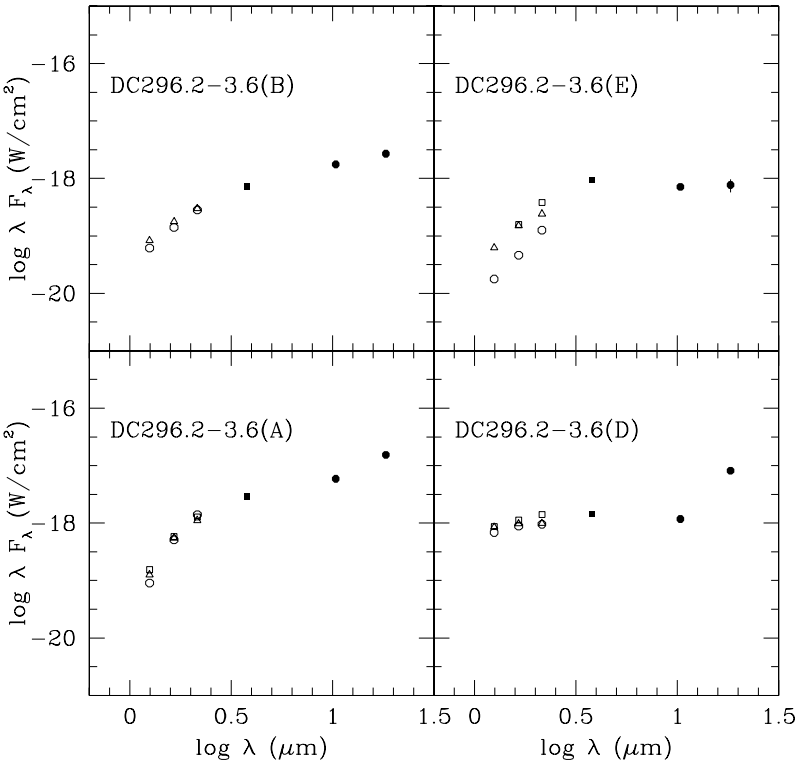

Figure 11. SEDs of sources A, B, D, and E in DC 296.2−3.6. The open and filled circles are the observations taken with the Baade and Gemini telescopes, respectively. The open triangles and squares are the near-IR photometry taken with the du Pont telescope and with 2MASS.

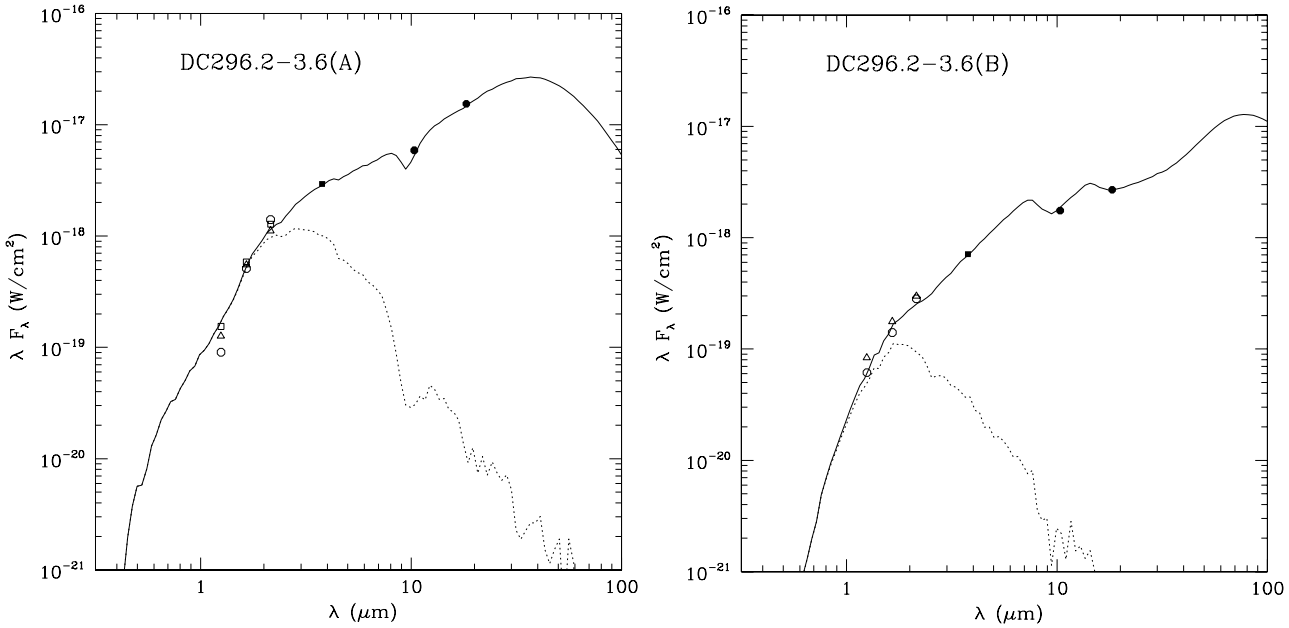

Figure 12. SED of the sources A and B. The best-fit models of the SEDs derived from the Robitaille et al. (2007) R07 fitting tool are over-plotted as solid lines. The dashed lines represent the stellar photosphere used as input to the radiation transfer code. The parameters of the models are given in Table 3.

quality of the fit of the model R07 by Robitaille et al. (2007) to their SEDs.

4. The presence of a number of young IR sources in DC 296.2−3.6 supports the hypothesis by Henning & Launhardt (1998) that the *IRAS* sources in the far Carina arm are cores of DC complexes with embedded low-mass star clusters.

This work is based partially on observations made with the European Southern Observatory telescopes obtained from the ESO/ST-ECF Science Archive Facility. M.T. acknowledges support from PAPIIT/UNAM grant No. IN102803.

Facilities: Las Campanas Observatory (PANIC), Gemini South (T-ReCS).

REFERENCES

Bessel, M. S., & Brett, J. M. 1988, PASP, 100, 1134
Bourke, T. L., Hyland, A. R., Robinson, G., James, S. D., & Wright, C. M. 1995, MNRAS, 276, 1067
Brand, J., & Blitz, L. 1993, A&A, 275, 67
Brand, J., Blitz, L., & Wouterloot, J. G. A. 1986, A&AS, 65, 537
Cohen, M., Walker, R. G., Carter, B., Hammersley, P., Kidger, M., & Noguchi, K. 1999, AJ, 117, 1864
Egan, M. P., Price, S. D., Moshir, M. M., Cohen, M., & Tedesco, E. 1999, Tech. Rep. AD-381933; AFRL-VS-TR-1999-1522
Hartley, M., Manchester, R. N., Smith, R. M., Tritton, S. B., & Goss, W. M. 1986, A&AS, 63, 27
Henning, Th., & Launhardt, R. 1998, A&A, 338, 223
Lynds, B. J. 1962, ApJS, 7, 1
Meyer, M. R., Calvet, N., & Hillebrand, L. A. 1997, AJ, 114, 288
Moorwood, A., et al. 1998, Messenger, 94, 7
Persi, P., Ferrari-Toniolo, M., Busso, M., Origlia, L., Robberto, M., Scaltriti, F., & Silvestro, G. 1990, AJ, 99, 303
Persi, P., Tapia, M., Roth, M., Gómez, M., & Marenzi, A. R. 2007, Mem. Soc. Astron. Ital., 78, 673
Persson, S. E., West, S. C., Carre, D. M., Sivaramakrishnan, A., & Murphy, D. C. 1992, PASP, 104, 204
Rieke, G. K., & Lebofsky, M. J. 1985, ApJ, 288, 618
Robitaille, T. P., Whitney, B. A., Indebetouw, R., & Wood, K. 2007, ApJS, 169, 328
Stetson, P. B. 1987, PASP, 99, 101